Experimental Study on Performance Improvement of Underwater Acoustic Communication Using a Single Vector Sensor

Kang-Hoon Choi, Jee Woong Choi, Sunhyo Kim, Peter H. Dahl, David R. Dall'Osto, and Hee Chun Song

***Abstract*—Underwater acoustic communication is heavily influenced by intersymbol interference caused by the delay spread of multipaths. In this article, communication sequences transmitted from a drifting source were received by a fixed acoustic vector receiver system consisting of an accelerometer-based vector sensor and a pressure sensor, which can measure the three-directional components of vector quantity and pressure at a point. The underwater acoustic communication experiment was conducted in water approximately 30 m deep off the south coast of Geoje Island, South Korea, in May 2017 during the Korea Reverberation Experiment. Acceleration signals received by the vector sensor were converted to pressure-equivalent particle velocities, which were then used as input for a four-channel communication system together with acoustic pressure. These four channels have multipaths with different amplitudes but the same delay times, providing directional diversity that differs from the spatial diversity provided by hydrophone arrays. To improve the communication performance obtained from directional diversity, the Multichannel Combined Bidirectional Block-based Time Reversal Technique was used, which combines bidirectional equalization with time-reversal diversity and block-based time reversal that was robust against time-varying channels. Communication performance was compared with the outcomes produced by several other time reversal techniques. The results show that the Multichannel Combined Bidirectional Block-based Time Reversal Technique using a vector sensor achieved superior performance under the environmental conditions considered in this article.**

***Index Terms*—Bidirectional block-based time reversal (BiBTR), directional diversity, particle velocity channel, single vector sensor.**

Manuscript received 27 October 2022; revised 23 July 2023 and 13 December 2023; accepted 18 February 2024. This work was supported by the Agency for Defense Development, South Korea, under Grant UD200010DD. The work of Peter H. Dahl, David R. Dall'Osto, and Hee Chun Song was supported by The U.S. Office of Naval Research. *(Corresponding author: Jee Woong Choi.)*

Associate Editor: C. C. Tsimenidis.

Kang-Hoon Choi is with LIG Nex1, Seongnam 13488, South Korea (e-mail: kanghoon.choi@lignex1.com).

Jee Woong Choi is with the Department of Marine Science and Convergence Engineering / Department of Military Information Engineering, Hanyang University ERICA, Ansan 15588, South Korea (e-mail: choijw@hanyang.ac.kr).

Sunhyo Kim is with the Maritime Security Research Center, Korea Institute of Ocean Science and Technology, Busan 49111, South Korea (e-mail: sunhyo@kiost.ac.kr).

Peter H. Dahl and David R. Dall'Osto are with the Applied Physics Laboratory, University of Washington, Seattle, WA 98105 USA (e-mail: dahl@apl.washington.edu; dallosto@apl.washington.edu).

Hee Chun Song is with the Scripps Institution of Oceanography, La Jolla, CA 92093-0238 USA (e-mail: hcsong@ucsd.edu).

Digital Object Identifier 10.1109/JOE.2024.3374424

I. Introduction

IN SHALLOW water, acoustic communication channels are subject to large multipath spread due to multiple interactions with ocean boundaries, causing intersymbol interference (ISI). The multipath channels have time-varying characteristics due to temporal variations of ocean environments. Especially, when a communication platform is moving, the communication channel has a low coherence time and undergoes a frequency shift due to the Doppler effect [1], [2]. The time-varying multipath channel produces time-varying ISI and phase distortion, which results in significant degradation of coherent acoustic communication performance. To overcome these problems, various communication techniques, such as multichannel decision-feedback equalizer (DFE) [3], [4], [5] and multichannel time reversal (TR) combining with DFE [1], [6], [7], [8], [9] have been studied for decades, because these techniques normally take advantage of gains in spatial diversity, a spatially separated receiver array is needed. However, accommodating a receiver array in a compact underwater communication platform can be difficult.

An acoustic vector sensor can simultaneously measure acoustic pressure and the orthogonal components of acoustic vector quantities, such as acoustic acceleration or particle velocity, at a single position in space [10], suggesting an alternative to receiver arrays for compact communication platforms. Several studies have verified the effectiveness of underwater communication system that use a vector sensor through simulations and experiments [11], [12], [13], [14]. For the receiver arrays, the acoustic pressure signals received by each channel exhibit multipath characteristics with different delay times and amplitudes, resulting in spatial diversity gain. Vector signals, such as acoustic particle velocity signals and acceleration signals, received from a single vector sensor also exhibit multipath characteristics with different amplitudes, but each multipath has the same delay time. Therefore, when a single vector sensor is used, the communication performance can be improved through the channel gain provided by the directionalities of each channel (i.e., directional diversity gain) rather than spatial diversity because a single vector sensor measures four different components at a single location.

Although a single vector sensor is spatially efficient, performance improvement can be relatively low compared with the receiver array due to the same delay time of the multipaths. In this article, a bidirectional block-based time reversal (BiBTR) [15] technique is applied and demonstrated using a single vector

sensor while the source is drifting, in an effort to improve the communication performance exploiting the directional diversity provided by a single vector sensor. The BiBTR technique combines bidirectional decision-feedback equalization (BiDFE) [16], [17], [18], [19] and block-based time reversal (BTR) technique [2], [20], [21], [22], [23]. The TR technique improves communication performance by mitigating ISI and increasing the signal-to-noise ratio (SNR) through temporal and spatial focusing. In addition, the BTR technique updates the communication channel block-by-block, using detected symbols from the preceding block. This process operates under the assumption that the channel remains nearly time-invariant within each block [2], [20], [21], [22], [23]. BiDFE utilizes time-reversal diversity that combines the soft outputs produced by forward and backward DFEs [19]. The communication performance produced by combining the directional diversity of the particle velocity channels and the time-reversal diversity of BiBTR technique was verified with data collected from a vector sensor during the Korea Reverberation Experiment (KOREX-17).

II. Experimental Description

Underwater acoustic communication experiments using a single vector sensor were conducted in shallow waters off the south coast of Geoje Island in South Korea on 25 May 2017, as part of KOREX-17 [24], [25], [26]. An omni-directional transducer (D/11, Neptune Sonar Limited, Kelk, United Kingdom) was used as an acoustic source, which was deployed at a depth of 13 m from the *R/V Mirae* operated by the Agency for Defense Development, South Korea, and drifted away from the receiver at an average speed of approximately 0.6 kn while transmitting communication signals. The transmitted signals were measured by an acoustic vector receiver (M20, GeoSpectrum Technologies, Dartmouth, Canada) deployed by the Applied Physics Laboratory, University of Washington. This receiver consisted of an acoustic pressure sensor and an accelerometer-based vector sensor having a frequency range of 1 Hz–3 kHz, which was positioned 1 m above the bottom at a depth of 29 m, as shown in Fig. 1(a). The accelerometer-based vector sensor has the capability to measure two horizontal components (x and y) and one vertical component (z) of the acoustic acceleration signals. The horizontal distance between the vector receiver and the acoustic source, measured by a global positioning system (GPS850, AscenKorea, South Korea), increased from 143 to 670 m with time along the trajectory shown in Fig. 1(b). The sound speed profile, as measured using conductivity-temperature-depth (CTD) casts (AML, Oceanographic, Canada), was nearly constant with depth over the duration of the experiment, as indicated in Fig. 1(c).

Surficial sediment samples were taken from the bottom using a grab sampler near the vector receiver. The mean grain size of the sediment samples was 5.7ϕ (where $\phi = -\log2(\mathrm{d}/\mathrm{d}_0)$, d is the grain diameter in millimeters, and d_0 is a reference length of 1 mm), which corresponds to silt. The surficial sediment sound speed at the experimental site was expected to be approximately 1568 m/s, based on the empirical relationship between the mean grain size and sediment sound speed [27]. During the experiment, sea-surface waves were measured by a directional waverider (DWR-G4, Datawell, Netherlands) moored at the experimental site, and the root-mean-square (rms) wave height was approximately 0.08 m, indicating calm seas.

The communication packet consisted of a probe signal followed by a communication sequence. The probe signal was a 100 ms-long linear frequency modulated (LFM) pulse in a frequency band of 2.5–3.5 kHz, which was used to synchronize the communication sequence. The communication sequence was a quadrature phase shift keying (QPSK)-modulated signal lasting 8 s, with a carrier frequency of 3 kHz and a symbol rate of 500 symbols per second and consisting of 4000 symbols containing a sequence of training symbols prior to information symbols. The training symbol with a length (N_T) of 400 symbols (0.8 s) was used for Doppler shift estimation, channel estimation, and equalization. A root-raised cosine pulse with a roll-off factor of 1 was employed as a pulse-shaping filter to mitigate the effects of time sampling errors induced by Doppler shift in our experiment environment where the source is in motion. The baseband sampling rate for the demodulation process into symbols was set equal to the symbol rate.

III. BiBTR Communication Using a Single Vector Sensor

Because an acoustic vector sensor can simultaneously measure the orthogonal components of vector quantity and acoustic pressure with different SNR ratios and channel characteristics, it can be used as a receiver in a single input multiple output system for underwater communication. In this article, the communication sequences were received by an accelerometer-based vector sensor capturing the x, y, and z components of the acoustic acceleration. The received acoustic acceleration signals of each component were then converted to pressure-equivalent particle velocities $p_i(t)$ using the following equation [11], [28]:

$$p_i\ (t) = -\rho_0 c \int_0^t a_i\,(\tau)\,d\tau \tag{1}$$

where $a_i(\tau)$ is the acoustic acceleration signals of the x, y, and z components. ρ_0 and c are the water density and the speed of sound in water, respectively.

As mentioned in Section I, the three components of particle velocity have multipath characteristics that differ only in amplitude because the propagation angle of a multipath is different in each component, but the delay time is the same. Therefore, unlike a spatially separated receiver array having the spatial diversity gain of different amplitudes and delay times, when a single vector sensor is used, only the directional diversity can produce the channel gain.

To improve the performance of underwater acoustic communication using a single vector sensor in ocean environment that dynamically changes in both space and time, we used BiBTR technique, which combines BTR technique and BiDFE. In BiDFE, combination of the soft outputs of forward and backward DFEs creates time-reversal diversity [17] to reduce error propagation caused by incorrect decision of feedback in DFE. Several studies of BiDFE combined with TR using receiver arrays have been conducted [15], [29]. Song [15] demonstrated

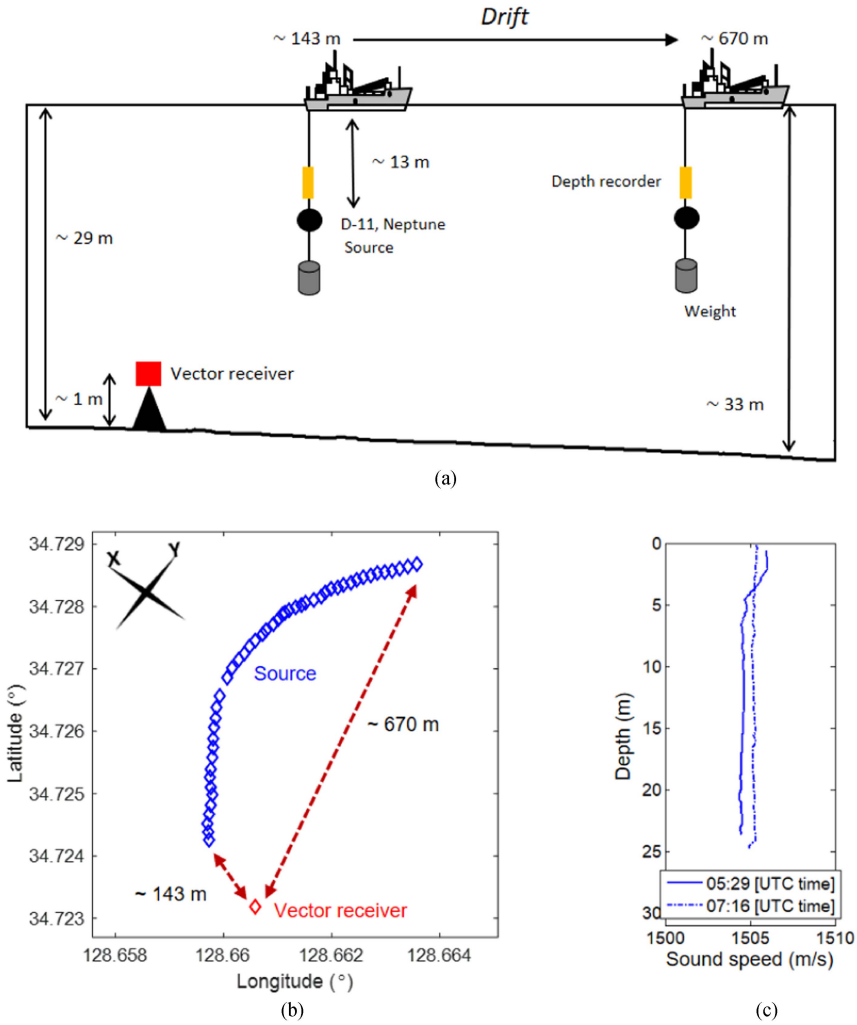

Fig. 1. (a) Experimental layout of the underwater acoustic communication using a vector receiver system, (b) trajectory of the acoustic source drifting away from the receiver position, and (c) sound speed profiles in the water column measured by CTD casts.

that BiDFE combined with TR techniques, such as passive time reversal (PTR) and BTR techniques, improved the communication performance by 0.4 to 1.8 dB in output SNR depending on the time-varying characteristics of communication channels, compared with TR techniques alone, despite the necessity to double the number of training symbols. In addition, it was more beneficial when applied to time-varying channels.

Fig. 2 depicts a block diagram of BiBTR technique using the acoustic pressure and pressure-equivalent particle velocity signals, $p_i[n]$ as inputs. The subscript i represents 1 to 4, meaning the pressure, x, y, and z components of particle velocity, in that order. BiBTR comprises forward BTR and backward BTR, and each BTR involves multichannel TR combining and a single-channel DFE consisting of a feedforward filter and a feedback filter. The TR combining improves symbol detection performance in the DFE by preemptively reducing ISI. The output $\tilde{d}$ of BiBTR is obtained as a weighted linear summation of the soft outputs $\tilde{d}_f$ in the forward BTR and the reversed version of the soft outputs $\tilde{d}_b$ in the backward BTR, as follows [17]:

$$\tilde{d}\ [n] = \beta \tilde{d}_f\,[n] + (1-\beta)\,\tilde{d}_b\,[n]\,,\ n = 1, \ldots, N, \qquad (2)$$

where β is the weighting factor $(0 \le \beta \le 1)$ and N is the total symbol number. Song [15] used $\beta = 0.5$ as an optimal value for TR communications. In this study, we exhaustively investigated the communication performance of BiBTR using β values between 0 and 1, and the performance was also optimal at β values near 0.5.

PTR technique compresses a communication signal in the time domain using a channel estimated by the probe signal or training symbols transmitted prior to an information-bearing communication signal, assuming that the channel is time invariant. However, because an underwater acoustic communication channel varies with time, performance deteriorates if the duration of the communication signal is relatively long compared with the temporal variation of the ocean environment. BTR technique compensates for time-varying channels by dividing them into blocks within the communication sequence using a time window within which the channels can be assumed to be time-invariant and then updating the channels block by block [2], [20], [21], [22], [23]. Fig. 3 depicts the receiver structure of BTR communication using a single vector sensor, which consists of noise normalization, block-by- BTR, multichannel combining,

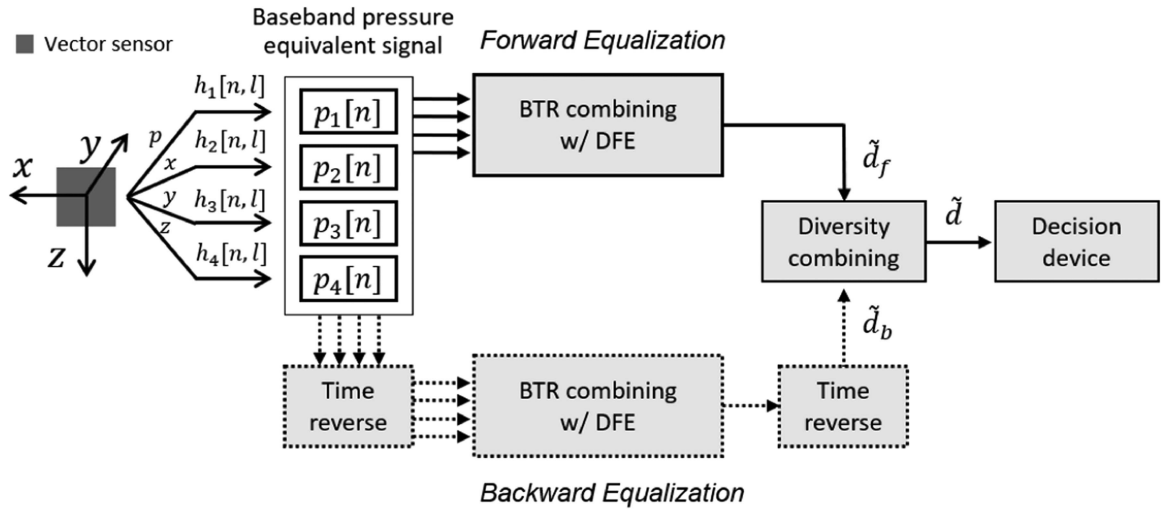

Fig. 2. Block diagram for BiBTR technique using a single vector sensor, which combines the soft outputs of the forward BTR and backward BTR. The four channels used for input are acoustic pressure and the pressure-equivalent x, y, and z particle velocity signals.

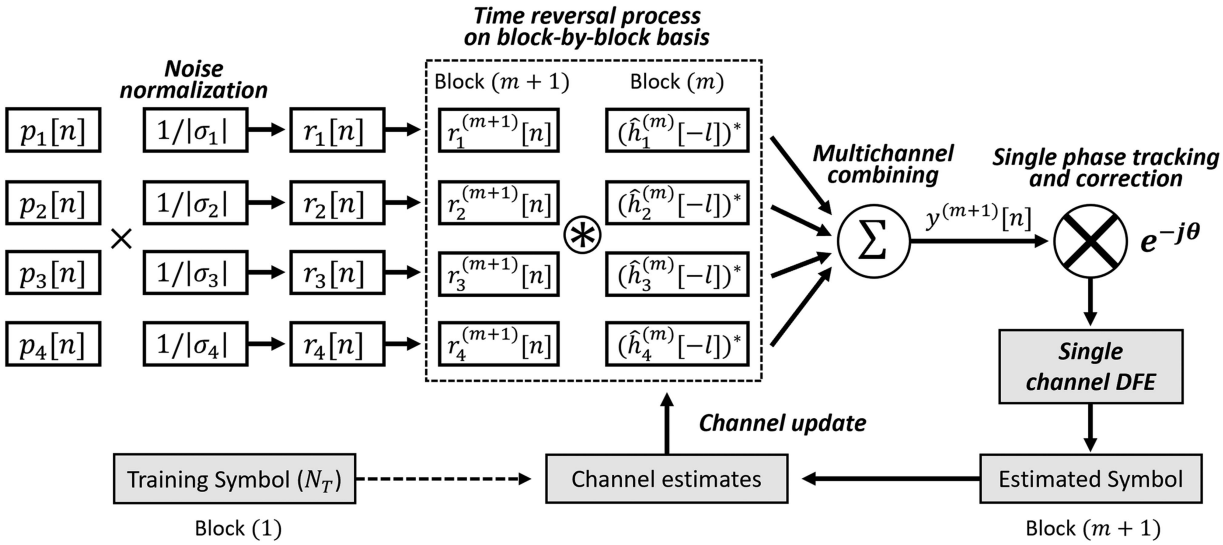

Fig. 3. Block diagram for the receiver structure of BTR technique using a vector sensor. TR for each channel is performed block by block, and the results are combined. The process for phase tracking and correction is performed between a TR combining process and single-channel DFE.

single phase tracking and correction, single-channel DFE, and a channel update.

Due to the difference in noise power between acoustic pressure and pressure-equivalent particle velocities measured at the same point [30], Song et al. [11] conducted noise normalization before the demodulation process in BTR communication. This methodology enhances the output SNR by adjusting the signal powers of particle velocities in relation to the reciprocal of the nonuniformly distributed noise powers among pressure and particle velocities. In this study, the noise powers in the acoustic pressure and particle velocity signals ${\sigma_i}^2$ were estimated from the noise signals before the communication signals were received. Noise-normalized signals $r_i[n]$ were used as inputs for multichannel TR combining on a block-by-block basis.

The baseband channels of each block for TR were estimated by a matching pursuit (MP) algorithm. MP is an algorithm that selectively estimates significant taps by using an optimal fit between source symbols and received symbols and is usually applied to estimate communication channels with a sparse nature, such as underwater acoustic channels [23], [31]. In this article, the total length of the multipath and the number of significant taps within the multipath were calculated using the channel impulse responses estimated from the matched filtering output of the LFM signal. Specifically, the significant tap number was determined by considering only impulses within -10 dB of the impulse from the peak energy among the multipath. The tap number was utilized to estimate the baseband channel for MP algorithm. Subsequently, taps that exhibited insignificance were assigned a value of zero.

In the next step, to apply the TR process to each block, the channels $\hat{h}_i^{(1)}[l]$ of pressure and particle velocities, estimated by the training symbol corresponding to the first block ($m = 1$),

were first reversed in time and subsequently convolved with the symbols within the second block ($m = 2$) $r_i^{(2)}[n]$. The TR-processed symbols within the second block were subsequently multichannel combined using the following equation:

$$\begin{aligned} y^{(2)}[n] &= \sum_{i=1}^{4} \left(r_i^{(2)}[n] \circledast \left(\hat{h}_i^{(1)}[-l] \right)^* \right) \\ &= s^{(2)}[n] \circledast \sum_{i=1}^{4} \left(h_i^{(2)}[n,l] \circledast \left(\hat{h}_i^{(1)}[-l] \right)^* \right) \\ &\quad + \sum_{i=1}^{4} \left(z^{(2)}[n] \circledast \left(\hat{h}_i^{(1)}[-l] \right)^* \right) \\ &= s^{(2)}[n] \circledast q^{(2)}[n,l] + w^{(2)}[n] \end{aligned} \tag{3}$$

where $h_i^{(2)}[n,l]$ is the actual time-varying channel for the second block, l is the symbol index in time, $s^{(2)}[n]$ and $z^{(2)}[n]$ are the source symbol and noise component,t respectively, for the second block, and $q^{(2)}[n,l]$ and $w^{(2)}[n]$ are the multichannel-combined q-function and noise component respectively for the second block. The superscript $*$ and the symbol $\circledast$ denote the conjugate and convolution operator, respectively. The q-function, the sum of the correlations between the actual and estimated channels, is representative of the effective impulse response after TR and is nearly symmetrical with respect to the main lobe [15].

After TR combining of the second block ($m = 2$), single-phase tracking and correction processes were performed prior to DFE to allow the DFE to focus primarily on removing residual ISI. The symbols estimated by the DFE output for the second block were used to update the channel estimates, which were applied to the symbols within the third block ($m = 3$) for TR. These processes were iterated sequentially within the communication sequence.

Phase tracking was conducted using a decision-feedback (decision-directed) phase-locked loop (DFPLL) based on the maximum-likelihood (ML) estimate [32] prior to the DFE, as illustrated in Fig. 3. The ML algorithm estimates signal parameters, such as carrier phase, by maximizing the likelihood function. In this article, the carrier phase was estimated by taking the inverse tangent of the ratio of two correlation outputs. These outputs were derived from cross-correlating the source symbols (or estimated symbols) with the received symbols and averaging the results over 20 symbols. The phase tracking was carried out using known training symbols and then using the estimated symbols in the decision-directed mode.

As the acoustic source drifts, communication signals exhibit continuously changing multipath delay characteristics due to spatial and temporal variations in the ocean environment. Consequently, the filter length in the DFE must be tailored to the channel's characteristics. In this article, the length of the feedforward filter was determined based on the delay time corresponding to approximately 97% of the accumulated energy of the multipath [33]. The length of the feedback filter was set to half the feedforward filter length. Adaptive updating of the filter tap weights in the DFE was accomplished using a recursive least-squares algorithm with a forgetting factor of 0.99 [32].

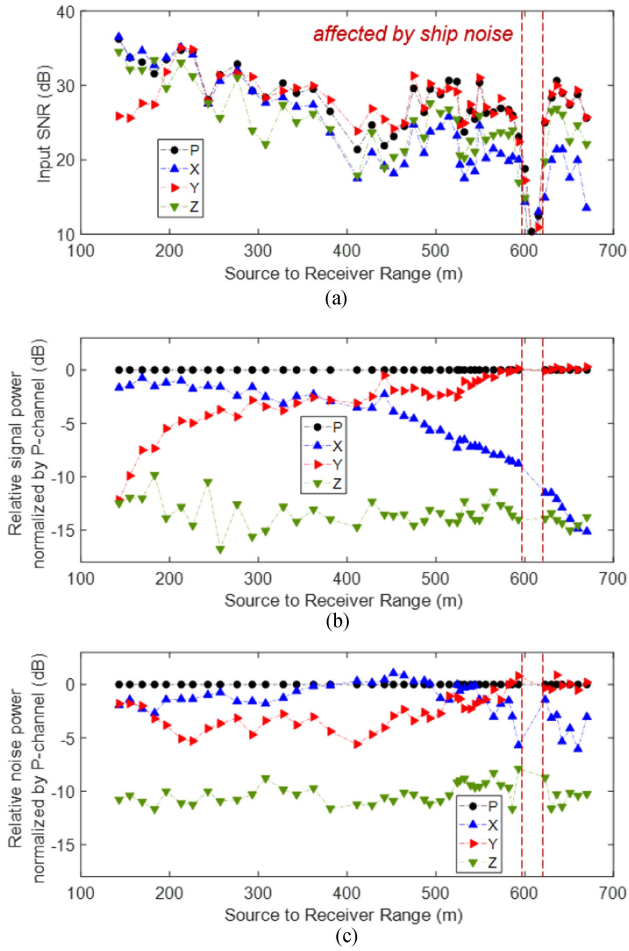

Fig. 4. (a) Input SNR as a function of range for the P, X, Y, and Z channels. (b), (c) Signal power and noise power of the particle velocity channel in baseband signal, respectively, normalized by that of the pressure channel corresponding to each range.

IV. Communication Results

A. Channel Characteristics of Acoustic Pressure and Particle Velocities

Fig. 4(a) depicts the input SNRs for the channels corresponding to the pressure and x, y, and z components of the pressure-equivalent particle velocity (hereafter referred to as the P, X, Y, and Z channels), which were estimated using the power ratio between the communication channel and the background noise in the baseband for each channel. As the acoustic source drifted away from the vector receiver, the input SNR decreased gradually, with the source–receiver range between approximately 1 and 12 dB per channel. There were exceptions at approximately 600 m from the receiver, shown in the red dashed box, in which the SNR decreased dramatically due to ship noise from an unknown vessel passing above the receiver. Signals corresponding to this area were therefore excluded from the communication performance analysis.

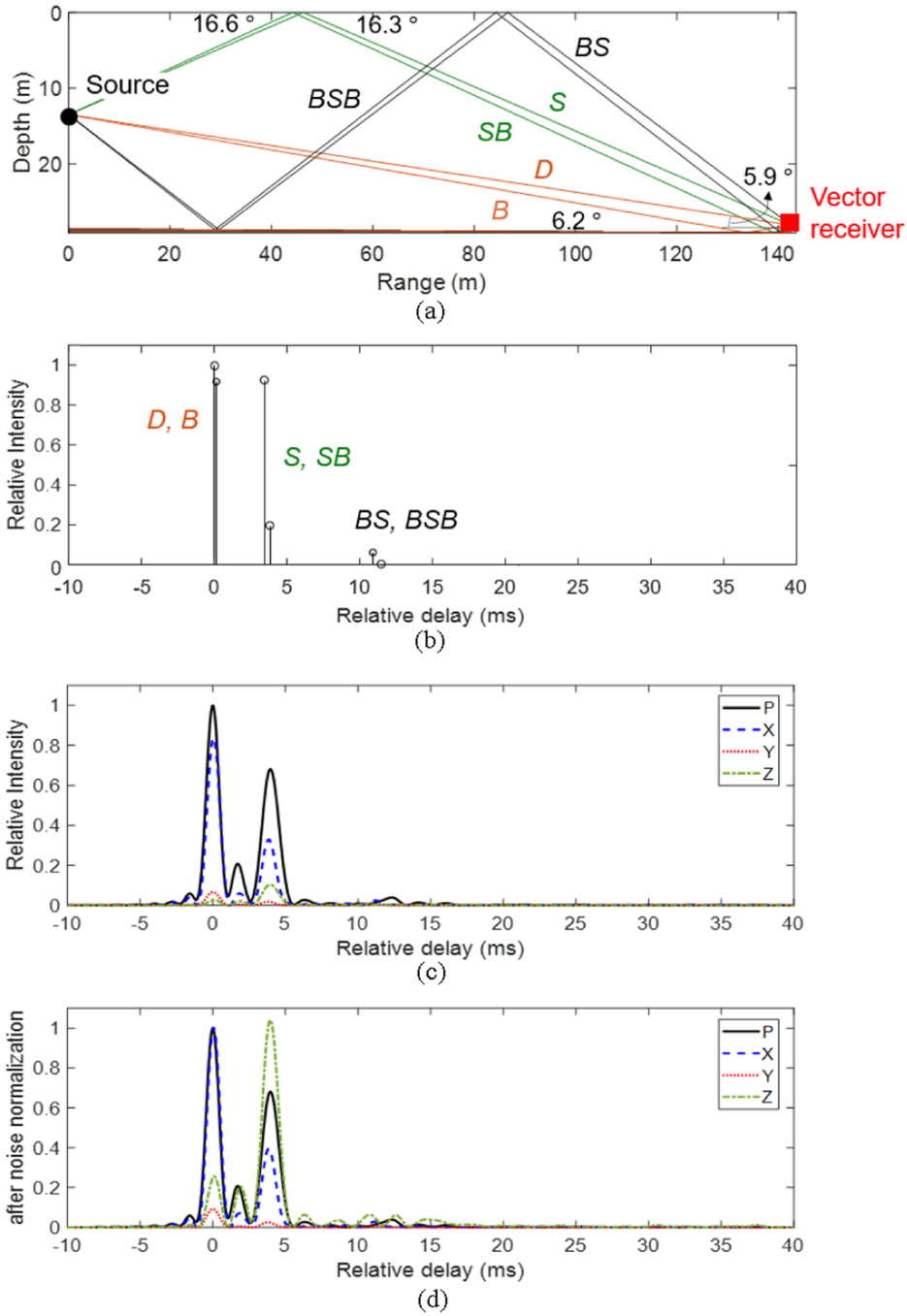

Fig. 5. (a) Eigenray tracing output and (b) channel impulse response for the first six arrivals predicted at a source–receiver range of 143 m. (c), (d) Channel impulse responses of the P, X, Y, and Z channels before and after noise normalization, respectively, which were estimated by matched filtering of LFM signal.

Fig. 4(b) shows the relative signal power of the X, Y, and Z channels compared with the signal power of the P channel as a function of the source–receiver range for the signals before noise normalization in BTR. The relative signal power of each channel was assessed by utilizing the impulse with the highest energy among the multipath in the baseband, and it was normalized by that of the pressure channel at each range. As the range increased, the relative signal power of the X channel decreased while that of the Y channel increased, which is consistent with the change in direction according to the trajectory of the acoustic source shown in Fig. 1(b). The signal powers in the Z channel were smaller than those of the P channel by more than 10 dB. The signal powers of the X and Y channels intersected at approximately 380 m, at which point it can be expected that the source was positioned at 45° from the azimuth with respect to the vector receiver.

Fig. 4(c) shows the relative noise powers of the X, Y, and Z channels compared with the noise power of the P channel as

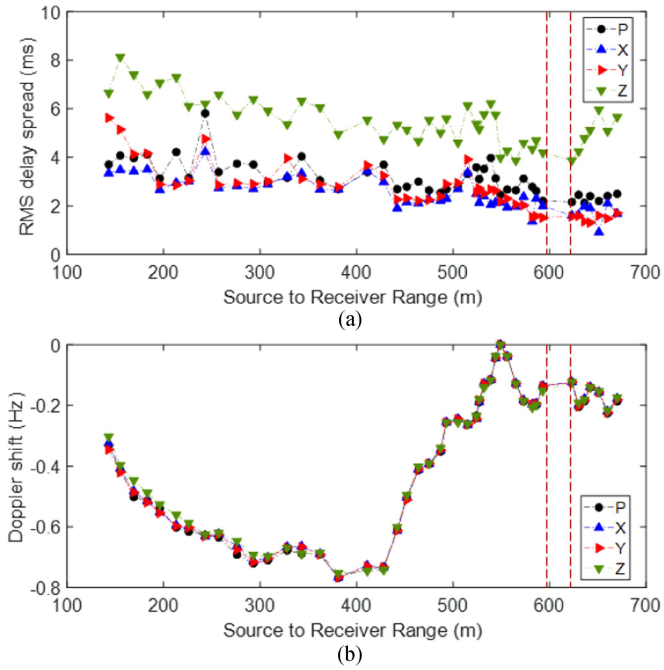

Fig. 6. (a) RMS delay spreads and (b) Doppler shifts of the P, X, Y, and Z channels estimated for all source–receiver ranges.

a function of range for the noise before noise normalization in BTR. The relative noise power of each channel was estimated from the noise signal preceding the communication signal in the baseband, and it was normalized by that of the pressure channel at each range. The noise powers of the X and Y channels were similar to or a marginally lower than those of the P channel, but the noise powers in the Z channel were an average of 13 dB lower than those of the P channel. As there was a significant difference in the noise power of each channel, noise normalization was performed using the noise power of each channel to use for multichannel TR combining.

Fig. 5(a) and (b) depicts the eigenray tracing output and channel impulse response corresponding to the first six arrivals predicted by Bellhop [34], a ray-based propagation model for the P channel at a source–receiver range of 143 m. The main arrival structure consisted of direct (*D*), bottom (*B*), sea surface (*S*), and surface–bottom (SB) paths in this order. For this geometry, the bottom grazing angles of the *B* and SB paths were predicted by the Bellhop propagation model to be 6.4° and 17.0°, respectively, and the corresponding bottom losses were predicted to be 0.6 and 3.4 dB, respectively, according to the Rayleigh bottom loss model [35], for a homogeneous fluid half-space, using sound speed, density, and attenuation in sediment obtained through the empirical relationship with mean grain size [27]. In contrast, the bottom grazing angle of the BS path was predicted to be 27.1°, and the corresponding bottom loss was predicted to be 9.4 dB, which was significantly higher than those of the early arrivals. The first arrival group consisted of the *D* and *B* paths, and the second arrival group consisted of the *S* and SB paths. However, the two paths in each group were not time-resolved because the receiver was just 1 m above the bottom. As mentioned earlier, the channel impulse responses corresponding to the P, X, Y, and Z channels had the same delay times, but different amplitudes (because each path was received with a different angle of arrival).

Fig. 5(c) and (d) shows the channel impulse responses of the P, X, Y, and Z channels as estimated before and after noise normalization for the signals, respectively. During the noise normalization process, the adjustment of signal powers based on the disparity in noise power between particle velocities and acoustic pressure induced noticeable alterations in the channel impulse responses of particle velocities. In particular, given the significantly lower noise power in the Z channel compared with the P channel, noise normalization resulted in an increase in the signal power of the Z channel by the difference in noise power between the two channels. After noise normalization, the relative intensity of the first group of the X channel increased by that of the P channel, while in the second group, the relative intensity of the Z channel surpassed those of the other channels. In addition, in shallow water, the later arrivals, the stronger the vertical component. Accordingly, in the case of the Z channel, ISI energy received after the second arrival group tended to increase, resulting in a greater delay spread compared with the other channels, as shown in Fig. 6(a).

The rms delay spread σ_τ is a parameter indicating the extent of time spread due to the difference in arrival times of multipaths, a major communication performance factor that can estimate the degree of ISI, and can be defined as [36]

$$\sigma_\tau = \sqrt{\frac{\sum_l |h[l]|^2 \tau_l^2}{\sum_l |h[l]|^2} - \left(\frac{\sum_l |h[l]|^2 \tau_l}{\sum_l |h[l]|^2}\right)^2} \tag{4}$$

where $h[l]$ and τ_l are the baseband channel impulse response and its delay time at the lth symbol index, respectively. Fig. 6(a) shows rms delay spreads of the P, X, Y, and Z channels for all source–receiver ranges. The rms delay spreads for all channels tend to decrease gradually as the range increases. Overall, the X and Y channels showed rms delay spreads similar to those of the P channel, but the Z channel showed more than twice as long rms delay spreads in all ranges. From this result, it was expected that the Z channel would be significantly more affected by ISI compared with other channels. The Doppler shift is caused primarily by relative movement between the source and receiver. The mean Doppler shift f_D during one communication sequence can be estimated from the Doppler power spectrum [37]

$$f_D = \frac{\sum_k P_D[k] f_k}{\sum_k P_D[k]} \tag{5}$$

where $P_D[k]$ and f_k are the Doppler power spectrum and frequency shift corresponding to the kth frequency shift index, respectively. The Doppler power spectrum can be obtained by integrating the scattering function over the time delay [38]. Fig. 6(b) depicts the Doppler shifts estimated as a function of range. The Doppler shift varied within the range of -0.8 Hz to 0 Hz as the source–receiver range increased. The Doppler shift caused by the movement of the source and receiver also varied by almost same value in all channels, which is consistent with a previous report [39].

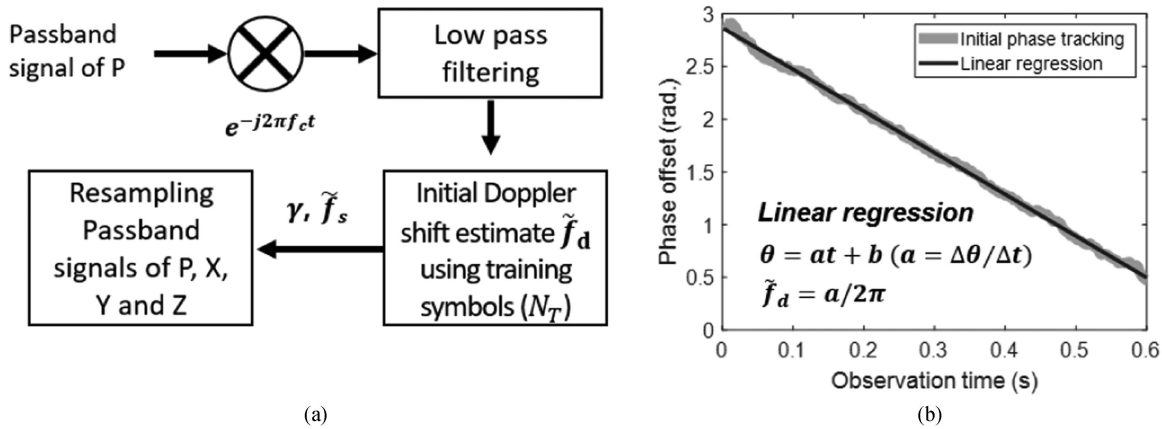

(a) (b)

Fig. 7. (a) Block diagram of the resampling process for the passband signal and (b) example of phase tracking using training symbols for the initial Doppler shift estimate.

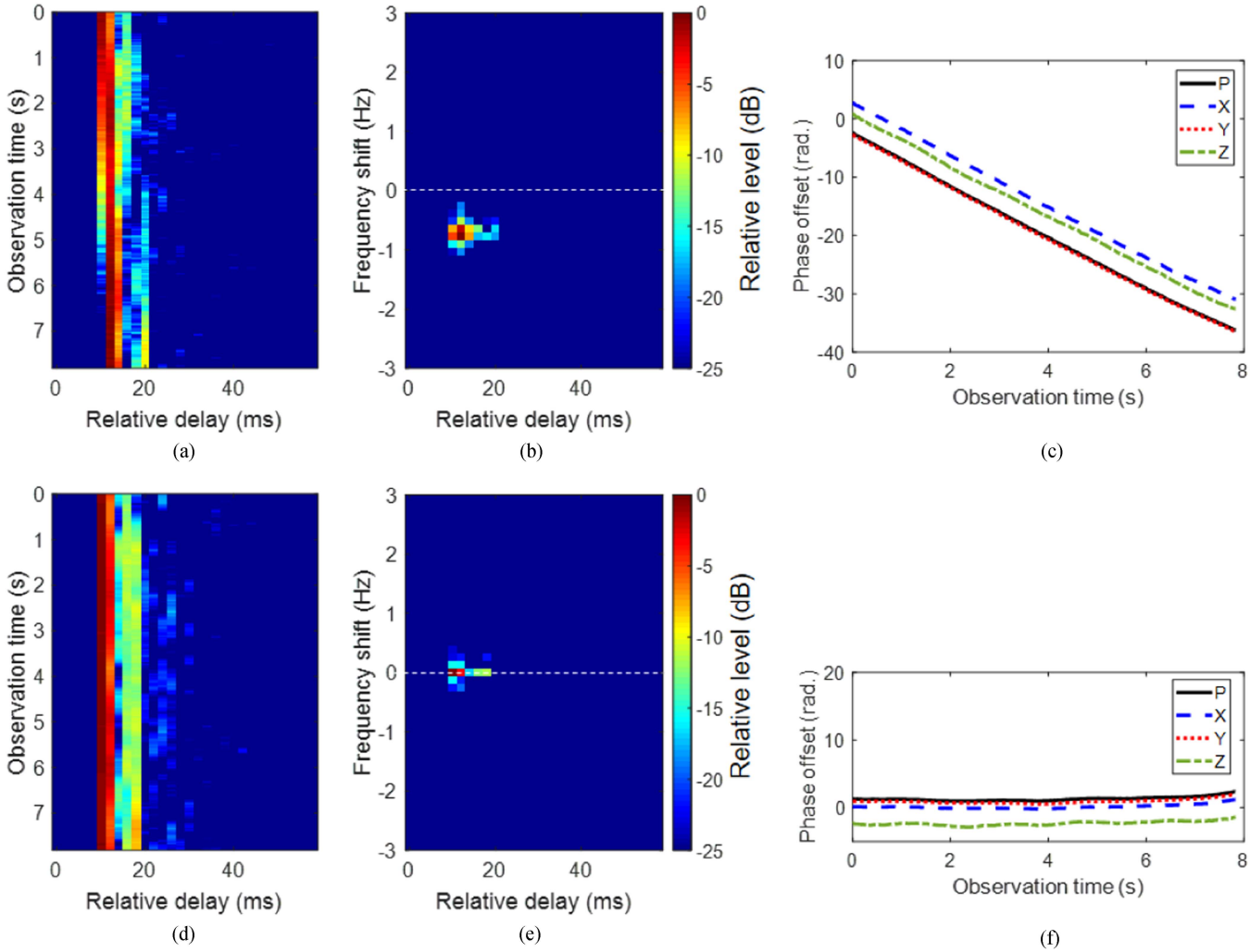

(a) (b) (c)

(d) (e) (f)

Fig. 8. (a) Baseband channel impulse response, (b) scattering function of the P channel, and (c) phase variations for the P, X, Y, and Z channels with observation time before resampling. The source–receiver range was approximately 308 m and, in this case, the Doppler shift was estimated to be −0.71 Hz. (d)–(f) Results estimated after resampling.

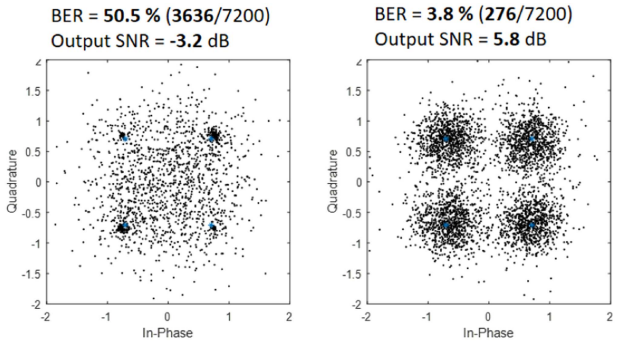

Fig. 9. Comparison of communication performance obtained by PTR using the P channel with a Doppler shift of −0.71 Hz at source–receiver range of ∼308 m (a) without and (b) with resampling.

TABLE I
AVERAGE CORRELATION COEFFICIENT VALUES OF CHANNEL IMPULSE RESPONSE AND NOISE BETWEEN ACOUSTIC PRESSURE AND PARTICLE VELOCITIES ACROSS ALL SOURCE–RECEIVER RANGES

	P and X	P and Y	P and Z
Average correlations of channel impulse response	0.93	0.92	0.76
Average correlations of noise	0.55	0.39	0.30

Correlations between pressure and the three particle velocity channels were investigated across all source–receiver ranges. Table I presents the average correlation coefficient values between each channel. In terms of the channel impulse response, the average correlations of the P channel with the X and Y channels consistently exceeded 0.90 at all ranges, while the average correlation with the Z channel was estimated to be around 0.7. Regarding the noise component, the average correlations of the P channel with the X, Y, and Z channels were 0.55, 0.39, and 0.30, respectively.

B. Communication Performance

When the acoustic source and/or receiver moves while transmitting and receiving a communication signal, the carrier frequency of the communication signal shifts, resulting in a change in the symbol interval and thus deterioration of communication performance [2]. A resampling process is therefore required to compensate for the Doppler shift. In this article, the Doppler shifts of the carrier frequency were corrected for the passband signal through resampling, which prevented distortion of the symbol detection interval due to the Doppler shift in the baseband signal.

A block diagram of the resampling process in passband signal is shown in Fig. 7(a). First, the communication signal at the P channel was multiplied by e^{-j2pif_ct} and then low-pass filtered to demodulate it into a complex baseband symbol. The initial phase tracking is then conducted using training symbols. After estimating a linear regression line for the phase tracking output, the initial value of the Doppler shift $\tilde{f}_d$ was calculated from the slope a of the regression line as $\tilde{f}_d = a/2\pi$, as shown in Fig. 7(b). Next, the modified sampling rate $\tilde{f}_s$ was obtained by γf_s, where f_s is the original sampling rate and γ is the resampling ratio given by $(f_c + \tilde{f}_d)/f_c$, where f_c is the carrier frequency. The passband signals of the P, X, Y, and Z channels were then resampled using a modified sampling rate to compensate for the Doppler shift. When the Doppler shift varies with time, a residual Doppler shift occurs even after the resampling process due to a difference between the initial Doppler shift $\tilde{f}_d$ and the time-varying Doppler shift. DFPLL was used to compensate for the residual Doppler shift and the resulting phase.

Fig. 8 illustrates the difference before and after the resampling process for the communication signals received at a source–receiver range of approximately 308 m. Without resampling, as the source moved away from the receiver, channel arrivals in the baseband channel impulse response moved to the next symbol in 3–5 s of observation time, as shown in Fig. 8(a). A Doppler shift of approximately −0.71 Hz can be seen in the scattering function illustrated in Fig. 8(b), and the phase varied with the observation time, as shown in Fig. 8(c). After resampling, the channel delays, Doppler shift, and phase variation were all significantly corrected as shown in Fig. 8(d)–(f), respectively.

To confirm the improvement in communication performance through resampling alone in the communication channel in which the Doppler shift occurs, PTR was performed for the P channel, with a Doppler shift of −0.71 Hz at a source–receiver range of approximately 308 m. The communication performance was analyzed as bit error rate (BER) and output SNR (SNR_o). The output SNR was calculated from the reciprocal of the mean-square error between the source symbol ($d[n]$) and estimated symbol ($\tilde{d}[n]$) as follows [9]:

$$\mathrm{SNR}_o = 10\log_{10}\left(|d[n]|^2 / E\left[\left|d[n] - \tilde{d}[n]\right|^2\right]\right) \quad (6)$$

where $E[\,]$ and $|\ |$ denote expectation and absolute values, respectively.

Fig. 9(a) and (b) shows the communication performances obtained by PTR without and with resampling process, respectively. The resampling process compensated for the carrier frequency shift and the channel delay variation, greatly improving communication performance. However, even after the resampling process, the communication performance showed the result of a BER of 3.8% and an output SNR of 5.8 dB due to the influence of the residual time-varying channel caused by spatio-temporal variations in the ocean environment.

Now, we employ BTR for the demodulation of the communication signals. In this article, the time window for the block in BTR was set to 400 ms (equivalent to 200 symbols), taking into account the minimum value of the coherence times of particle velocity channels across all ranges. Fig. 10(a) illustrates the communication performance achieved by a single-channel BTR for the P channel with resampling. The results indicate a significant improvement (approximately 2 dB) compared with the outcomes of a single-channel PTR with resampling depicted in Fig. 9(b), achieving a BER of 1.6% and an output SNR of 7.7 dB. Second, we applied multichannel combined BTR using

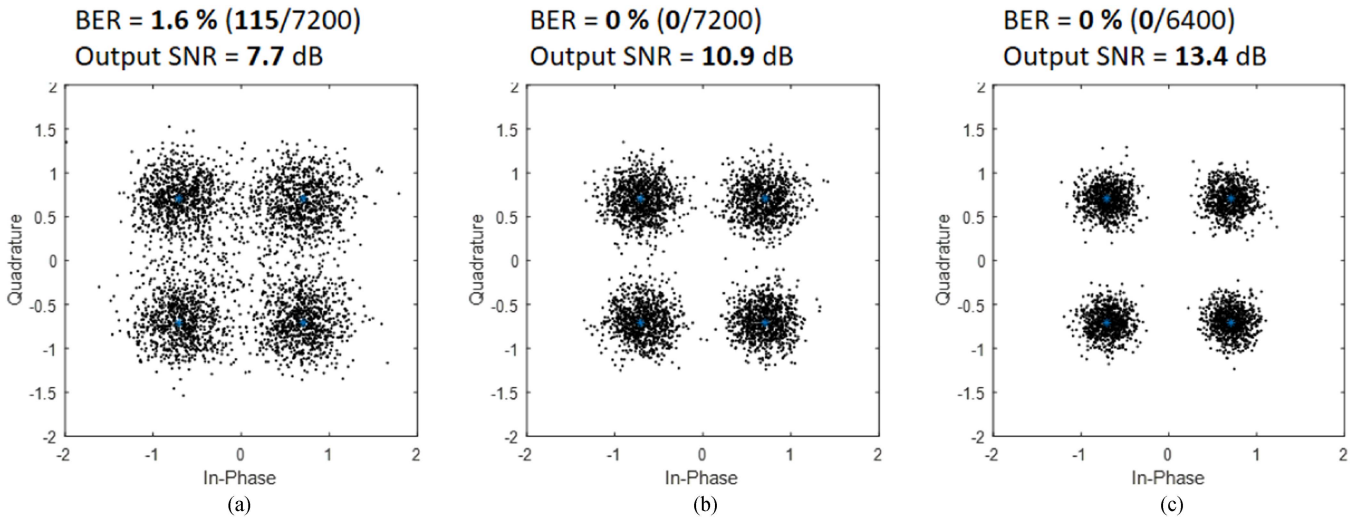

Fig. 10. Comparison of communication performances obtained by (a) BTR using the P channel, (b) multichannel combined BTR for the P, X, Y, and Z channels, and (c) multichannel combined BiBTR for the P, X, Y, and Z channels. The resampling process was included in the BTR and BiBTR techniques. The communication signal received at a source–receiver range of approximately 308 m was used, with an estimated Doppler shift of −0.71 Hz.

the P, X, Y, and Z channels. The result was error-free, with a 3.2 dB increase in output SNR compared with single-channel BTR, as indicated by Fig. 10(b). Last, multichannel combined BiBTR was performed. Although BiBTR lost 400 information symbols (800 bits for QPSK) because it requires doubling the training symbols, the performance further improved, with a 2.5 dB increase in output SNR compared with multichannel combined BTR, as shown in Fig. 10(c).

We investigate the communication performances for all source–receiver ranges. Fig. 11(a) shows the difference in Doppler shift as a function of range estimated using the P channel before and after resampling. The Doppler shifts were compensated for by the resampling process. However, residual Doppler shifts were still evident at ± 0.2 Hz due to the difference between the Doppler shifts estimated from the training symbols and those in the information symbols. Fig. 11(b) plots the output SNR as a function of range for different TR techniques. The cases of the short ranges with relatively large Doppler shifts confirmed the importance of resampling. In addition, the multichannel combined BiBTR achieved the best performance in all ranges.

Fig. 12(a) and (b) are distribution histograms of performance improvement by directional diversity and time-reversal diversity, respectively. The improvement in performance due to directional diversity was estimated from the difference in output SNRs between the multichannel combined BTR and the single-channel BTR using the P channel. For the source–receiver geometries used in this study, the directional diversity by the vector receiver system improved the output SNR by an average of 2.3 dB and up to 5.2 dB, as shown in Fig. 12(a). Next, the performance improvement due to time-reversal diversity was investigated by examining the difference in output SNRs between multichannel combined BiBTR and multichannel combined BTR; the time-reversal diversity improved the output SNR by 0.4 to 3.5 dB (an average of 2.0 dB) in all geometry cases, as depicted in Fig. 12(b).

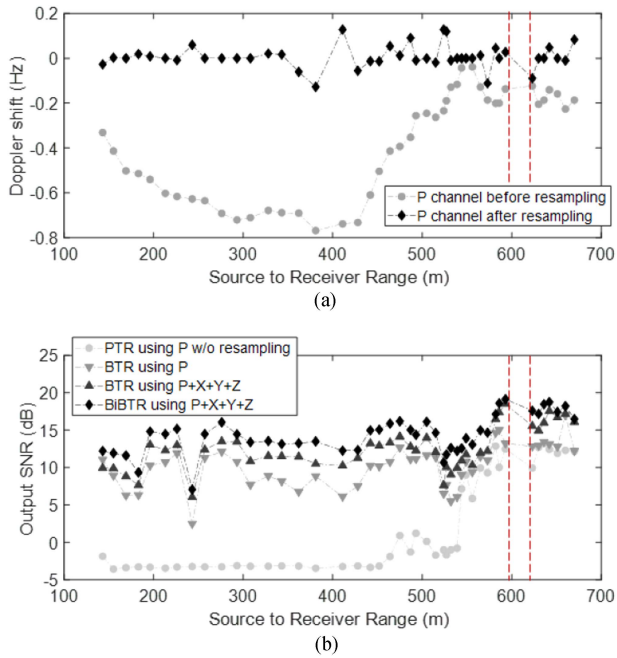

Fig. 11. Comparisons of (a) Doppler shifts for the P channel estimated before and after resampling and (b) communication performances in terms of the output SNR obtained by PTR using the P channel without resampling (•), BTR using the P channel (▼), multichannel combined BTR (▲), and multichannel combined BiBTR (♦).

V. Discussion and Summary

The effectiveness of underwater communication in shallow water using a single vector sensor was investigated. A vector sensor can simultaneously measure three-directional components of acoustic vector quantities from a single position in space. The vector sensor may therefore be a useful alternative to hydrophone arrays, which are bulky and less space-efficient. The

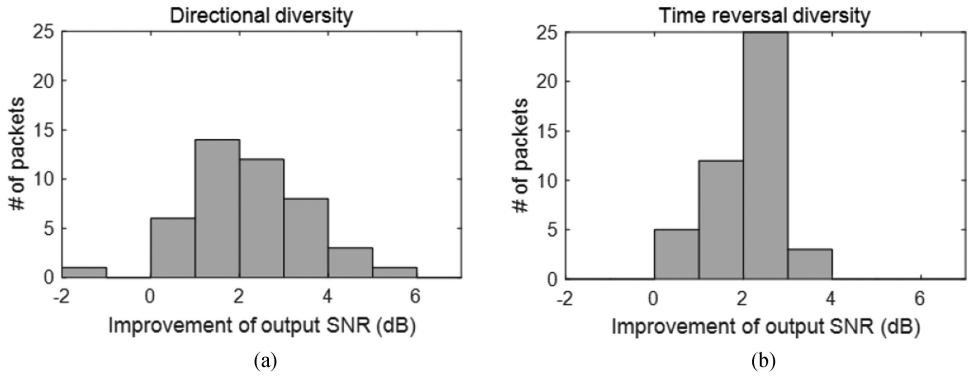

Fig. 12. Distribution histograms of output SNR increments improved by (a) directional diversity and (b) time-reversal diversity.

single vector receiver system used in the experiment consisted of an accelerometer-based vector sensor and an acoustic pressure sensor. The three-directional components of the acoustic acceleration signals were converted to three components of pressure-equivalent particle velocities, which were used as inputs for four-channel combined TR techniques for demodulation of communication signals with an acoustic pressure signal.

A hydrophone array receives acoustic pressure signals from hydrophones at spatially distinct locations. Therefore, the signal received on each channel exhibits multipath characteristics with different delay times and amplitudes, resulting in spatial diversity gain. Since the P, X, Y, and Z channels measured by a single vector receiver system have different amplitudes but the same delay time, this diversity can be referred to as "directional diversity." The directional diversity is generated by a difference in the directionality of the received signal, which differs from the spatial diversity of a hydrophone array and may have a weaker gain than the spatial diversity gain. We applied BiBTR technique to the demodulation of communication signals received by our vector receiver system. Because BiBTR technique uses combinations of soft outputs of forward and backward DFEs, it can benefit from time-reversal diversity despite requiring a doubling of training symbols at the front and back of the communication sequence.

The underwater communication experiment was conducted in shallow waters off the south coast of Geoje Island, South Korea in May 2017, as part of KOREX-17. The acoustic source transmitted communication packet signals consisting of LFM probe signal and QPSK communication sequence while drifting away from the receiver system over a distance of 143–670 m. The vector receiver system, consisting of an accelerometer-based vector sensor and a hydrophone, was located 1 m above a silty bottom at a depth of 29 m. Acoustic bottom interactions at this fine-grained sediment limited the number of dominant paths for the geometry considered in our experiment to the paths corresponding to one or two bottom interactions.

Doppler shifts in the communication signal received by the vector receiver system were due to the acoustic source drifting away from the receiver while transmitting the communication signals. The Doppler shift of the carrier frequency was corrected for the passband signal through resampling to prevent distortion of the symbol detection interval due to the Doppler shift in the baseband signal. Fig. 13(a) and (b), respectively, shows the communication performances of the PTR using only the P channel without and with resampling for all source–receiver ranges. The results confirmed that the communication performance improved significantly only through resampling.

The PTR technique requires the assumption that the channel is invariant for the duration of the communication packet. However, because the ocean environment is not frozen in time, the underwater communication channel also fluctuates rapidly with time, which can lead to deterioration in communication performance. BTR technique improves the performance of a time-varying channel by dividing communication sequences into blocks and updating the channels block by block. Fig. 13(c) shows the communication performance of BTR using the P channel. We confirmed that the performance was markedly superior to those shown in Fig. 13(a) and (b). Last, BiBTR technique was applied to obtain the gain by time-reversal diversity, and the results of the P, X, Y, and Z channels were combined to obtain the gain by directional diversity for all source–receiver ranges, as shown in Fig. 13(d). Four-channel combined BiBTR achieved the best performance, with a BER of 0.08% and an output SNR of 13.7 dB, demonstrating the efficiency of BiBTR using a vector sensor.

There existed a substantial disparity between the input and output SNRs. This discrepancy is likely attributed to the unaddressed movement of the acoustic source during drifting, resulting in a residual Doppler shift and a time-varying channel. Despite efforts to mitigate these effects through techniques, such as resampling and BiBTR, complete elimination was not achieved. Note that resampling was based on the mean Doppler shift of all the acoustic paths, even though individual paths may exhibit slightly different Doppler shifts. There was also an issue concerning channel synchronization using the matched filter of the LFM signal, which was transmitted 1 s prior to the communication signal. This interval could induce a time sampling error due to the variability of synchronization time caused by Doppler effects.

The directivity index (DI) for a single vector sensor can be theoretically derived as approximately 6 dB $[= 10\log_{10}(4)]$ when optimal weighting is applied to each component for a

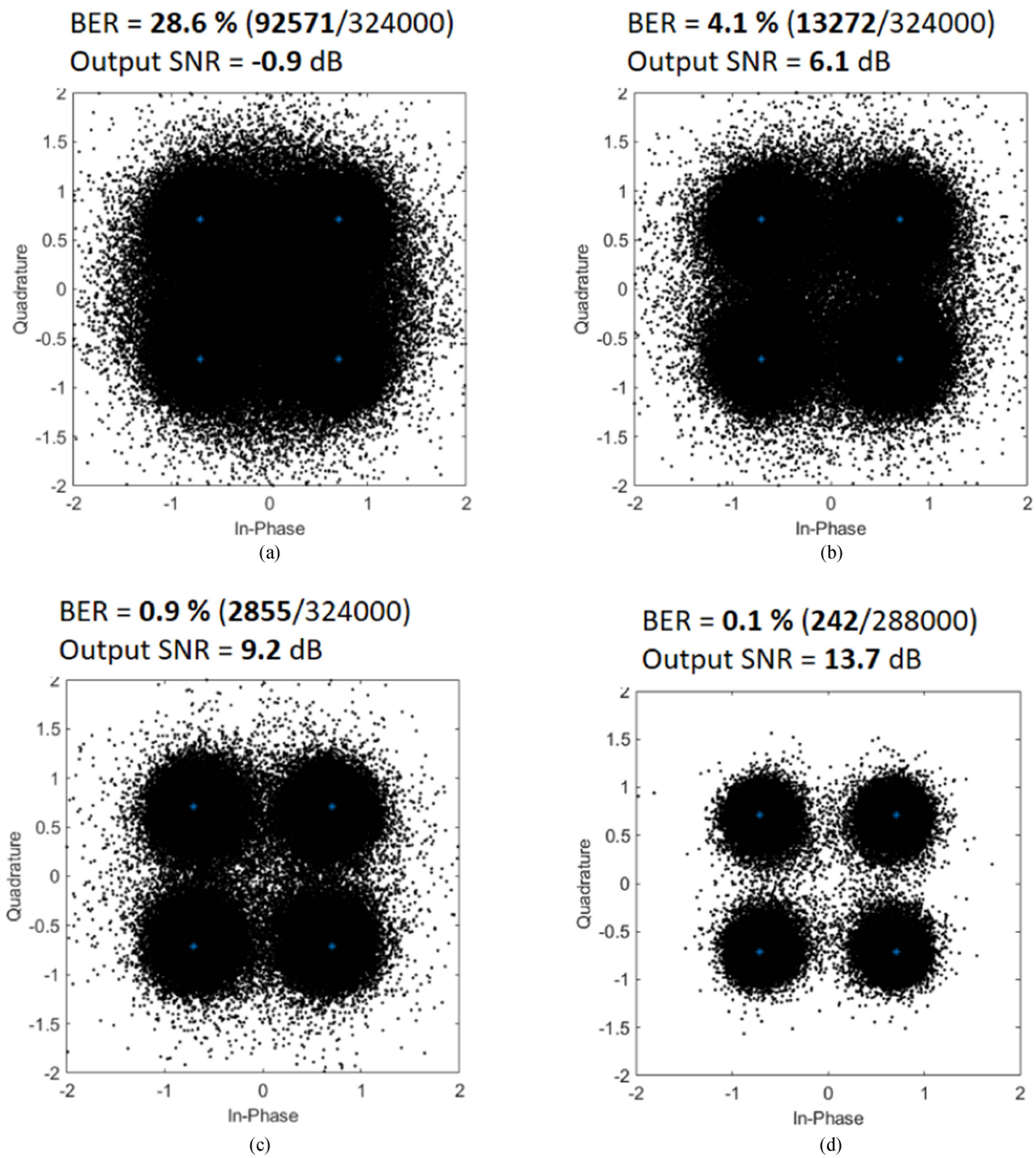

Fig. 13. Constellation plots of communication performances estimated for all source–receiver ranges using (a) a single-channel PTR without resampling, (b) single-channel PTR with resampling, (c) single-channel BTR with resampling, and (d) multichannel combined BiBTR with resampling.

single plane wave propagating in a homogeneous, isotropic noise environment [40]. In this article, optimal weighting was not utilized, but noise normalization was applied during the multichannel combining process to equalize the noise powers across channels. Further research will explore the factors influencing the enhancement in output SNR through the directional diversity of a single vector sensor in terms of DI.

Finally, although the usefulness of the vector sensor in underwater acoustic communication was verified, interpretation of the results of our experiment should take into account that the experiment was conducted only at source–receiver ranges of less than approximately 700 m in shallow water with silty sediment at a depth of approximately 30 m. Each component of the multipaths received by a vector sensor depends on geoacoustic parameters as well as geometry, including water depth, range between source and receiver, and their deployment depths. Since the acoustic interactions with the ocean bottom have a significant influence on multipath structure in shallow waters, and it affects the vertical and horizontal components of the vector quantities, and consequently the performance of underwater acoustic communication using the vector sensor. Further studies are needed to verify the usefulness of vector sensors for underwater acoustic communication in various ocean environments with different types of sediment and water depths.

ACKNOWLEDGMENT

This work was done during the doctoral studies of the first author with Hanyang University.

REFERENCES

[1] H. C. Song, "Peer-reviewed technical communication: An overview of underwater time-reversal communication," *IEEE J. Ocean. Eng.*, vol. 41, no. 3, pp. 644–655, Jul. 2016.
[2] H. C. Song, "Time reversal communication with a mobile source (L)," *J. Acoust. Soc. Amer.*, vol. 134, no. 4, pp. 2623–2626, 2013.
[3] M. Stojanovic, J. Catipovic, and J. G. Proakis, "Adaptive multichannel combining and equalization for underwater acoustic communications," *J. Acoust. Soc. Amer.*, vol. 94, no. 3, pp. 1621–1631, 1993.
[4] M. Stojanovic, J. Catipovic, and J. G. Proakis, "Reduced-complexity spatial and temporal processing of underwater acoustic communication signals," *J. Acoust. Soc. Amer.*, vol. 98, no. 2, pp. 961–972, 1995.
[5] M. Stojanovic, "Recent advances in high-speed underwater acoustic communication," *IEEE J. Ocean. Eng.*, vol. 21, no. 2, pp. 125–136, Apr. 1996.
[6] T. C. Yang, "Temporal resolutions of time-reversal and passive-phase conjugation for underwater acoustic communications," *IEEE J. Ocean. Eng.*, vol. 28, no. 2, pp. 229–245, Apr. 2003.
[7] T. C. Yang, "Correlation-based decision-feedback equalizer for underwater acoustic communications," *IEEE J. Ocean. Eng.*, vol. 30, no. 4, pp. 865–880, Oct. 2005.
[8] M. Stojanovic, "Retrofocusing techniques for high rate acoustic communications," *J. Acoust. Soc. Amer.*, vol. 117, no. 3, pp. 1173–1185, 2005.
[9] H. C. Song et al., "Spatial diversity in passive time reversal communications," *J. Acoust. Soc. Amer.*, vol. 120, no. 4, pp. 2067–2076, 2006.
[10] A. Nehorai and E. Paldi, "Acoustic vector-sensor array processing," *IEEE Trans. Signal Process.*, vol. 42, no. 9, pp. 2481–2491, Sep. 1994.
[11] A. Song, A. Abdi, M. Badiey, and P. Hursky, "Experimental demonstration of underwater acoustic communication by vector sensors," *IEEE J. Ocean. Eng.*, vol. 36, no. 3, pp. 454–461, Jul. 2011.
[12] C. Wang, J. Yin, D. Huang, and A. Zielinski, "Experimental demonstration of differential OFDM underwater acoustic communication with acoustic vector sensor," *Appl. Acoust.*, vol. 91, pp. 1–5, 2014.
[13] S. Kim, H. Kim, S. Jung, and J. W. Choi, "Time reversal communication using vertical particle velocity and pressure signals in shallow water," *Ad Hoc Netw.*, vol. 89, pp. 161–169, 2019.
[14] F. A. Bozzi and S. M. Jesus, "Joint vector sensor beam steering and passive time reversal for underwater acoustic communications," *IEEE Access*, vol. 10, pp. 66952–66960, 2022.
[15] H. C. Song, "Bidirectional equalization for underwater acoustic communication," *J. Acoust. Soc. Amer.*, vol. 131, no. 4, pp. EL342–EL347, 2012.
[16] S. Ariyavisitakul, "A decision feedback equalizer with time reversal structure," *IEEE J. Sel. Areas Commun.*, vol. 10, no. 3, pp. 599–613, Apr. 1992.
[17] J. Balakrishnan and C. Johnson Jr., "Time-reversal diversity in decision feedback equalization," in *Proc. Allerton Conf. Commun., Control Comput.*, Oct. 2000, pp. 1–10.
[18] J. Balakrishnan, "Time-reversal decision feedback equalizer and MIMO channel training," Ph.D. dissertation, Cornell Univ., Ithaca, NY, USA, 2002.
[19] J. Nelson, A. Singer, U. Madhow, and C. McGahey, "BAD: Bidirectional arbitrated decision-feedback equalization," *IEEE Trans. Commun.*, vol. 53, no. 2, pp. 214–218, Feb. 2005.
[20] A. Song, M. Badiey, H. C. Song, W. S. Hodgkiss, and M. Porter, "Impact of ocean variability on coherent underwater acoustic communications during KauaiEx," *J. Acoust. Soc. Amer.*, vol. 123, no. 2, pp. 856–865, 2008.
[21] H. C. Song, W. A. Kuperman, and W. S. Hodgkiss, "Basin-scale time reversal communications," *J. Acoust. Soc. Amer.*, vol. 125, no. 1, pp. 212–217, 2009.
[22] H. C. Song, W. S. Hodgkiss, and P. A. van Walree, "Phase-coherent communications without explicit phase tracking," *J. Acoust. Soc. Amer.*, vol. 128, no. 3, pp. 969–972, 2010.
[23] H. C. Song, "Time reversal communications in a time-varying sparse channel," *J. Acoust. Soc. Amer.*, vol. 130, no. 4, pp. EL161–EL166, 2011.
[24] D. Tang, B. T. Hefner, and T. Shim, "Assessment of the temporal and spatial dependence of reverberation mechanisms for KOREX-17," *J. Acoust. Soc. Amer.*, vol. 144, 2018, Art. no. 1686.
[25] B. T. Hefner, D. Tang, J. W. Choi, and T. Shim, "Rocky outcrops as clutter in mid-frequency reverberation measurements," *J. Acoust. Soc. Amer.*, vol. 144, 2018, Art. no. 1687.
[26] T. Shim, B. T. Hefner, S.-U. Son, Y. Na, and D. Tang, "Oceanographic effects on mid-frequency acoustics during KOREX-17," *J. Acoust. Soc. Amer.*, vol. 144, 2018, Art. no. 1687.
[27] D. R. Jackson and M. D. Richardson, *High-Frequency Seafloor Acoustics*. Berlin, Germany: Springer-Verlag, 2006.
[28] D. R. Dall'Osto, P. H. Dahl, and J. W. Choi, "Properties of the acoustic intensity vector field in a shallow water waveguide," *J. Acoust. Soc. Amer.*, vol. 131, no. 3, pp. 2023–2035, 2012.
[29] H. Kim, S. Kim, J. W. Choi, and H. S. Bae, "Bidirectional equalization based on error propagation detection in long-range underwater acoustic communication," *Jpn. J. Appl. Phys.*, vol. 58, 2019, Art. no. SGGF01.
[30] M. Hawkes and A. Nehorai, "Acoustic vector-sensor correlations in ambient noise," *IEEE J. Ocean. Eng.*, vol. 26, no. 3, pp. 337–347, Jul. 2001.
[31] S. Cotter and B. Rao, "Sparse channel estimation via matching pursuit with application to equalization," *IEEE Trans. Commun.*, vol. 50, no. 3, pp. 374–377, Mar. 2002.
[32] J. Proakis, *Digital Communications*. New York, NY, USA: McGraw-Hill, 2008.
[33] P. H. Dahl and J. W. Choi, "The East China Sea as an underwater acoustic communication channel: Measurements of the channel impulse response(U)," *Amer. US Navy J. Underwater Acoust.*, vol. 56, pp. 1–12, 2006.
[34] M. B. Porter and H. P. Bucker, "Gaussian beam tracing for computing ocean acoustic fields," *J. Acoust. Soc. Amer.*, vol. 82, no. 4, pp. 1349–1359, 1987.
[35] G. V. Frisk, *Ocean and Seabed Acoustics*. Englewood Cliffs, NJ, USA: Prentice-Hall, 1994.
[36] T. S. Rappaport, *Wireless Communications: Principles and Practice*. Englewood Cliffs, NJ, USA: Prentice Hall, 2002.
[37] A. F. Molisch and M. Steinbauer, "Condensed parameters for characterizing wideband mobile radio channels," *Int. J. Wireless Inf. Netw.*, vol. 6, no. 3, pp. 133–154, 1999.
[38] P. A. van Walree and M. Smedsrud, "A discrete-time channel simulator driven by measured scattering functions," *IEEE J. Sel. Areas Commun.*, vol. 26, no. 9, pp. 1628–1637, Dec. 2008.
[39] H. Guo, A. Abdi, A. Song, and M. Badiey, "Delay and Doppler spreads in underwater acoustic particle velocity channels," *J. Acoust. Soc. Amer.*, vol. 129, no. 4, pp. 2015–2025, 2011.
[40] G. L. D'Spain, J. C. Luby, G. R. Wilson, and R. A. Gramann, "Vector sensors and vector sensor line arrays: Comments on optimal array gain and detection," *J. Acoust. Soc. Amer.*, vol. 120, no. 1, pp. 171–185, 2006.

Kang-Hoon Choi received the Ph.D. degree in underwater acoustics from the Department of Environmental Marine Sciences, Hanyang University, Seoul, South Korea, in 2023.

Since 2023, he has been a Research Engineer with the Maritime Research and Development Laboratory, LIG Nex1, Seoul. His research interests include underwater acoustic communication, underwater acoustic sensor network, and underwater acoustic communication channel modeling.

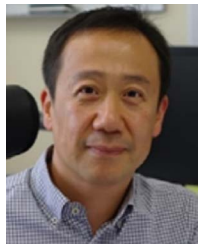

Jee Woong Choi received the Ph.D. degree in underwater acoustics from the Department of Earth and Marine Sciences, Hanyang University, Seoul, South Korea, in 2002.

From 2002 to 2007, he had been a Research Associate with the Applied Physics Laboratory, University of Washington, Seattle, WA, USA. Since 2007, he has been a Professor with the Department of Marine Science and Convergence Engineering, Hanyang University-ERICA, Ansan, South Korea. His main research interests include acoustic propagation in shallow water, geoacoustic inversion, underwater acoustic communication, and recently extended to target localization, and motion analysis.

Dr. Choi is a Fellow of the Acoustical Society of America and Vice President of the Acoustical Society of Korea.

Sunhyo Kim received the Ph.D. degree in underwater acoustics from the Department of Environmental Marine Sciences, Hanyang University, Seoul, South Korea, in 2016.

Since 2020, he has been a Senior Research scientist in the Marine Domain and Security Research Department, Korea Institute of Ocean Science and Technology, Busan, South Korea. His research interests include underwater acoustic communication, underwater acoustic sensor network, Naval oceanography, and underwater channel modeling.

Peter H. Dahl received the Ph.D. degree in ocean engineering from the Joint Program in Oceanography and Oceanographic Engineering, Massachusetts Institute of Technology, Cambridge, MA, USA, Cambridge/Woods Hole Oceanographic Institution, Woods Hole, MA, Joint Program in Oceanography and Oceanographic Engineering, in 1989.

He is currently a Senior Principal Engineer with the Applied Physics Laboratory, University of Washington, Seattle, WA, USA, where he is also a Professor of Mechanical Engineering. His research interests include experimental and modeling studies on intensity vector acoustics, shipping noise, and the underwater sound field from explosive sources including the effects on aquatic life.

Dr. Dahl is a Fellow of the Acoustical Society of America (ASA). He was the Chair of the ASA Technical Committee on Underwater Acoustics, the ASA Executive Council, and as ASA Vice President.

David R. Dall'Osto received the Ph.D. degree in mechanical engineering from the University of Washington, Seattle, WA, USA, in 2013.

He is currently a Senior Research Scientist and Engineer with the Applied Physics Laboratory, University of Washington. His research interests include modeling and measurement of acoustic intensity in the ocean and atmosphere, on both short-range and global scales. An important aspect of his research is the discovery of physical processes that produce structure in the intensity vector field, and validating such theoretical predictions through experiment.

Hee Chun Song received the Ph.D. degree in ocean engineering from the Massachusetts Institute of Technology, Cambridge, MA, USA, in 1990.

From 1991 to 1995, he was with the Korea Ocean Research and Development Institute, Ansan, South Korea. Since 1996, he has been a Research Scientist with the Marine Physical Laboratory, Scripps Institution of Oceanography, University of California San Diego, La Jolla, CA, USA. His research interests include time-reversed acoustics, waveguide physics, sonar array processing, and underwater acoustic communications.